Cosmic-ray deficit from the directions of the Moon and the Sun detected with the Tibet air-shower array

M. Amenomori,[a] Z. Cao,[b] L. K. Ding,[b] Z. Y. Feng,[c] K. Hibino,[d] N. Hotta,[e] Q. Huang,[c] A. X. Huo,[b] H. Y. Jia,[c] G. Z. Jiang,[c] S. Q. Jiao,[c] F. Kajino,[f] K. Kasahara,[g] Labaciren,[h] D. M. Mei,[h] L. Meng,[b] X. R. Meng,[h] Mimaciren,[h] K. Mizutani,[i] J. Mu,[j] H. Nanjo,[a] M. Nishizawa,[f] Nusang,[h] A. Oguro,[i] M. Ohnishi,[f] I. Ohta,[e] J. R. Ren,[b] To. Saito,[d] M. Sakata,[f] Z. Z. Shi,[b] M. Shibata,[k] T. Shirai,[g] H. Sugimoto,[l] X. X. Sun,[b] A. Tai,[j] K. Taira,[l] Y. H. Tan,[b] N. Tateyama,[g] S. Torii,[g] H. Wang,[b] C. Z. Wen,[c] Y. Yamamoto,[f] X. Y. Yao,[j] G. C. Yu,[c] P. Yuan,[b] T. Yuda,[d] J. G. Zeng,[c] C. S. Zhang,[b] H. M. Zhang,[b] L. Zhang,[j] Zhasang,[h] Zhaxiciren,[h] and W. D. Zhou[j]

(Tibet ASγ Collaboration)

[a]*Department of Physics, Hirosaki University, Hirosaki, Japan*
[b]*Institute of High Energy Physics, Academia Sinica, Beijing, China*
[c]*Department of Physics, South West Jiaotong University, Chengdu, China*
[d]*Institute for Cosmic Ray Research, University of Tokyo, Tanashi, Japan*
[e]*Faculty of Education, Utsunomiya University, Utsunomiya, Japan*
[f]*Department of Physics, Konan University, Kobe, Japan*
[g]*Faculty of Engineering, Kanagawa University, Yokohama, Japan*
[h]*Department of Mathematics and Physics, Tibet University, Lhasa, China*
[i]*Department of Physics, Saitama University, Urawa, Japan*
[j]*Department of Physics, Yunnan University, Kunming, China*
[k]*Faculty of Education, Yokohama National University, Yokohama, Japan*
[l]*Shonan Institute of Technology, Fujisawa, Japan*

(Received 25 August 1992; revised manuscript received 3 December 1992)

Data from the Tibet air-shower array were used to examine the cosmic-ray shadows of the Moon and the Sun at energies around 10 TeV. The shadowing effect was clearly observed at the 5.8σ level for the Moon, while the shadow of the Sun was found in the direction away from the Sun by 0.86° to the west and 0.43° to the south. The effect of the geomagnetic field has also been observed in the shadow of cosmic rays by the Moon. The observed deflection of the Sun's shadow is briefly discussed in connection with the effect of the magnetic fields between the Sun and the Earth. This is the first observation of the effects of such magnetic fields on the cosmic-ray shadow. The maximum-likelihood analysis of the Moon data set shows that the angular resolutions of the array for showers with its mode energies 7 and 35 TeV are $0.87°^{+0.13°}_{-0.10°}$ and $0.54°^{+0.11°}_{-0.08°}$, respectively.

PACS number(s): 96.40.Pq, 96.40.Kk, 96.50.Bh

I. INTRODUCTION

A detection of ultrahigh-energy (UHE) and/or very-high-energy (VHE) γ-ray signals from celestial point sources may give us a clue for understanding the acceleration of particles to ultrahigh energies. Since the first report on the detection of UHE γ rays from Cygnus X-3 by the Kiel group [1], many observations have been done on various sources including this. However, the majority of effort from discrete sources so far made has been reported just above the magic three-standard-deviations level [2], and the experiments are left exposed to the enormous backgrounds from hadronic showers.

In order to firmly establish the existence of point sources in this energy region, the quest for greater sensitivity of detector systems is therefore given top priority. In the TeV energy region, detailed imaging techniques of the Cherenkov light flash have been studied at the Whipple Observatory [3], and recently they succeeded in detecting TeV γ-ray signals from the Crab Nebula at the 20σ level, while no confirmation has been made by other observations at such significance. On the other hand, air-shower arrays are commonly used in the PeV energy region. The improvement in angular resolution based on accurate timing of the shower front is most powerful for isolating the small number of subset of showers arriving from the source direction, particularly in the light of claims for anomalous non-γ signals with abundant muons from Cygnus X-3 [1,4] or Hercules X-1 [5].

The detector system designed for improving the sensitivity for directional signals may have an opportunity to open a new research field in high-energy astrophysics. Clark [6] suggested in 1957 that the Sun and Moon must cast a shadow in the high-energy cosmic-ray flux and observation of their obscuration might give new information about the magnetic field of these bodies. Some sophisticated plans or ideas have been proposed so far. That is, shadowing of cosmic rays by the Moon through

the geomagnetic field could be used to measure the antiproton-proton ratio at TeV energies [7] or the average mass composition near 10^{14} eV, or more could be determined by observing the rigidity dependence of the onset of the Sun's shadow through the solar magnetic field [8].

In practice, the shadowing effects of the Moon and Sun by cosmic rays can be used to confirm the angular resolution of the air-shower array and to examine its systematic pointing errors. These analyses have been already done by several groups [9–11]. The Cygnus group [9] first measured the combined effect of the Sun and Moon at 100-TeV energies and found evidence at the 4.9σ level for a shadow at the predicted place.

The Tibet air-shower experiment [12] started in 1990 and aims at searching for celestial γ-ray point sources in the energy range from several TeV to PeV, with a good sensitivity. The site is located at Yangbajing (4300 m above sea level, 606 g/cm^2; 90.53° E, 30.11° N) in Tibet, China. The array is designed so as to achieve a good angular resolution better than 1° at energies around 10 TeV based on a Monte Carlo simulation. We have already reported the results on the search for steady emission of γ rays from the Crab Nebula, Cygnus X-3, and Hercules X-1 at energies around 10 TeV [13].

In this paper we study the shadowing of cosmic rays by the Moon and Sun at energies around 10 TeV in order to examine the angular resolution of the Tibet array. It is expected that cosmic-ray particles in this energy region are fairly affected by the geomagnetic field or the solar and interplanetary magnetic fields. We present the first observation of the shadowing of cosmic rays by the Sun under the influence of these magnetic fields.

Our plan in this paper is as follows. In Sec. II the experimental procedure is briefly reviewed. The experimental results on the shadowing of cosmic rays by the Moon and Sun are presented in Sec. III. Section IV is used for estimating the angular resolution of our air-shower array. Section V is devoted to summarizing the results.

II. EXPERIMENT AND ARRAY PERFORMANCE

The Tibet air-shower array has been in operation since January 1990 at Yangbajing. The fast-timing (FT) detector array consists of 45 scintillation detectors of 0.5 m^2 each, which are placed in a grid pattern of a 15-m spacing. This FT array is surrounded by 20 density detectors to obtain a good core location for each shower event. All the detectors are set in an inverted pyramidal style, and a lead plate of 5 mm thickness is put on top of each detector for converting γ rays in the air showers into electron pairs. In order to operate our system stably, some monitor systems are introduced. That is, a time-to-digital converter (TDC) tester module is used to calibrate all the TDC's at the start of every run. A laser system [14] is also incorporated to monitor the relative time-offset value, photomultiplier tube (PMT) gain, and linearity for each FT detector regularly. A rubidium clock and the GPS (global positioning system) provide information on the recording time of each event with sufficient accuracy. Data are stored on 8-mm video tape of 2.3 Gbyte capacity each by use of an EXB-8200 recorder.

Since June of 1990, our system has triggered the events at a rate of about 20 Hz under any fourfold coincidence in the FT detectors within a 300-ns time interval, where a discrimination level of each analogue-to-digital converter (ADC) is set to one particle per detector. About 5.3×10^8 events have been recorded during the period from June 1990 through October 1991. These data are used in the search for both the shadows of the Sun and Moon by high-energy cosmic rays.

The event selection was made imposing the following two conditions. First, each of the four FT detectors should give a signal more than 1.25 particles per 0.5 m^2. Second, among the four detectors which record the highest particle densities, two or more should be inside the central 5×5 detector matrix. It is found that about 50% of the total number of trigger events pass through these selection criteria.

In order to examine the performance of the array, a Monte Carlo simulation has been done by taking account of the experimental conditions. In this simulation the subroutine package GENAS [15] is employed. The primary particles are assumed to be protons with a differential power-law spectrum of the form of $E^{-\gamma}$, where γ changes from 2.73 to 3.00 at 2×10^{15} eV. The selection of the simulated showers is done under the same criteria as in the experiment.

Figure 1 shows the energy spectra of protons generating the showers which will be observed with the Tibet array. The upper histogram in this figure denotes the spectrum of protons producing the showers satisfying the selection criteria mentioned above, and the lower one is that of protons generating those with $\sum\rho_{FT}>100$, where ρ_{FT} denotes the shower particle density per square meters in each detector and the summation is taken over all the FT detectors. From this figure the mode energy of primary protons is estimated to be 7 TeV (the median energy is about 17 TeV) for all shower events and 35 TeV (56 TeV) for those with $\sum\rho_{FT}>100$.

For each Monte Carlo shower, we can estimate its ar-

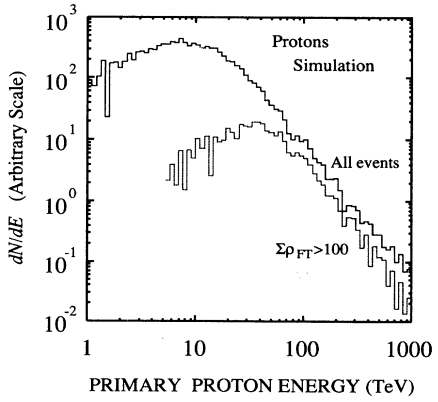

FIG. 1. Energy spectra of protons producing air showers to be observed with the Tibet array, obtained from the simulation. The upper histogram denotes the spectrum of protons producing air showers satisfying the selection criteria of all events (see text). The lower one is that of protons producing the showers with $\sum\rho_{FT}>100$.

rival direction with the same method as used in the experiment. The opening angle between the estimated direction and the given one is calculated for each of simulated showers. This opening angle distribution was used to estimate the angular resolution. Figure 2 shows the dependence of the opening angle on the shower size $\sum\rho_{FT}$ for proton-induced events. The simulation data are fitted by a straight line for each case, and they stand for the opening angles in which 20%, 50%, and 80% of events are contained at each shower size bin, respectively. It is seen that the opening angle decreases as $\sum\rho_{FT}$ increases. From this figure the angular resolution of the Tibet array, defined to be the half-angle of the cone containing 50% of events coming from a source direction, is estimated to be 1.15° for all proton-induced events and 0.49° for those with $\sum\rho_{FT} > 100$.

III. SHADOWING OF THE MOON AND SUN

The geocentric positions of the Sun in the sky were computed by taking account of the perturbations to the orbit of the Earth by the planets and Moon. Corrections for parallax were also made to the Moon coordinates. The error of the position calculation is estimated to be smaller than 0.02° for the Moon and 0.001° for the Sun. These values are much smaller than the angular resolution of the array and also than the apparent radii of the Moon and Sun.

Among 2.4×10^8 selected events used for the present analysis are the subsets of 1.09×10^6 events within 8° of the Sun and 1.24×10^6 events within 8° of the Moon and with the zenith angles less than 50°.

In the following analysis, we use a coordinate system fixed on the object (Moon or Sun), putting the origin of coordinates on its center. The position of each event observed is then specified by the angular distance θ and the position angle ϕ, where θ and ϕ are measured from the center and from the north direction, respectively. The event distributions plotted in such coordinate systems are used to examine the shadowing of cosmic rays by these objects. In order to measure a small decrease in event density, the background was carefully estimated for each object using the events which come from the following eight off-source positions. These positions (of feigned objects) are located on the same zenith angle as the Moon or Sun, but apart by ±5°, ±10°, ±15°, and ±20° in the azimuth angle. The average of the event densities around these eight off-source positions was taken to be the background, although some appropriate choices were made depending on the zenith angle. The background density distribution near the object is a function of θ and ϕ. Integrating this distribution on ϕ for each data set gives the angular density versus angular distance θ, all of which are well approximated by

$$F_{bg}(\theta) = -a\theta^2 + b \ . \quad (1)$$

The values of parameters a and b are given in Table I for each subset of data. The angular density distributions estimated depend weakly on the angular distance.

TABLE I. Summary of the parameter values appeared in Eq. (1).

	Moon		Sun	
	All	$\sum\rho_{RT} > 100$	All	$\sum\rho_{FT} > 100$
a (deg^{-4})	0.849	0.320	1.829	0.308
b (deg^{-2})	5749.68	783.54	6221.89	876.26

For the events observed around the Moon and Sun, the angular density versus angular distance was obtained by calculating the event densities for concentric rings with a width of 0.2° for each data set. The difference between this event density and the background one for each data set determines a deficit or number of missing events at an angle θ from the center. Figure 3 shows the deficit densities versus the angular distance from the center of the Moon and Sun for all events and for high-energy events with $\sum\rho_{FT} > 100$, respectively. The shadowing or cosmic-ray deficit is evident for the Moon. The value of χ^2 for an assumption of no deficit at $\theta < 1°$ (inner five angular bins) is calculated to be 34.3 for all events (the χ^2 probability is 8×10^{-7} or 4.8σ), and that at $\theta < 0.6°$ (inner three bins) for those with $\sum\rho_{FT} > 100$ is 15.94 (8×10^{-5} or 3.8σ). For all events of the Sun, however,

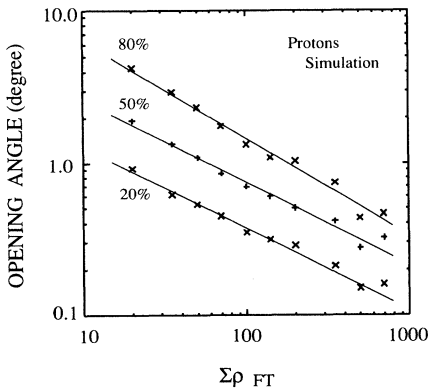

FIG. 2. Dependence of the opening angle on the air shower size $\sum\rho_{FT}$ for shower events induced by protons. Simulation results are fitted by a straight line for each, and they stand for the opening angles in which 20%, 50%, and 80% of events are contained at respective $\sum\rho_{FT}$, respectively.

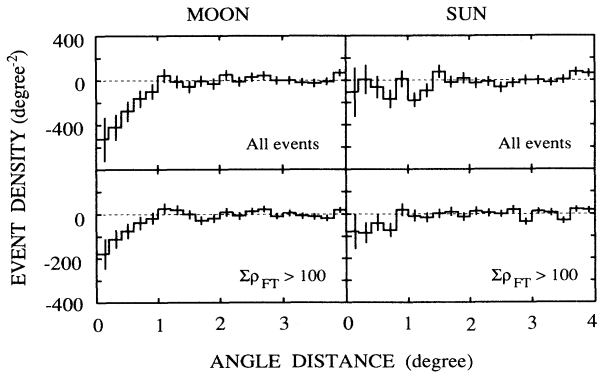

FIG. 3. Angular density of events vs angular distance from the Moon and Sun for all events and those with $\sum\rho_{FT} > 100$, respectively. The dotted lines show the background levels.

no clear deficit is seen just at the Sun's position, but some degree of the deficit is observed rather at the angular distance around $\theta=1.0°$ (the χ^2 probability for no deficit at $\theta<1.2°$ is 1.56×10^{-2} or 2.15σ). For high-energy events with $\sum\rho_{FT}>100$, the shadowing appears more clearly at the expected position, and the χ^2 probability for no deficit assumption at $\theta<0.8°$ (four angular bins) is calculated to be 4.3×10^{-3} (2.6σ).

In order to search for the actual position of the Sun's shadow, the arrival directions of cosmic-ray events were examined around the Sun using the subset of all events. For this, the area of $4°\times4°$ centered on the Sun was divided into 32×32 cells, each size being a $0.125°\times0.125°$, and a two-dimensional histogram was obtained of event densities per cell. The same histogram was also made for the background obtained above, while it was once smoothed out by taking a moving average on the event densities over 9×9 cells centered on each concerning cell. We then subtract this smoothed background from the event histogram. The deficit event density obtained at each cell was again smoothed out over 7×7 cells. Figure 4 shows the map of the event densities around the Sun thus obtained, giving the weight of the deficit of event density from the background. The weight is $(E-B)/\sqrt{E}$, where E and B are the event and background densities, repsectively. Contour lines start from 1σ deficit with a step of 1σ. It is well seen that the shadowing is observed in the direction away from the Sun to the west-southwest by about 0.9°.

Using the maximum-likelihood method, the most probable position of the center of the deficit is found at 0.86° to the west and 0.43° to the south when the angular resolution of the array is assumed to be 0.87° (see Sec. IV). The logarithm of likelihood is calculated to be 6.7 at this position, and the statistical significance for the shadow is calculated to be 3.7σ,[1] while the logarithm of likelihood is -12.7 at the actual solar position. Even with a trial factor as large as 1024 (total number of cells), the ratio of likelihoods between true and observed Sun positions times the trials factor would be 3.8×10^{-6}. Hence the observed displacement of the Sun's shadow is quite significant.

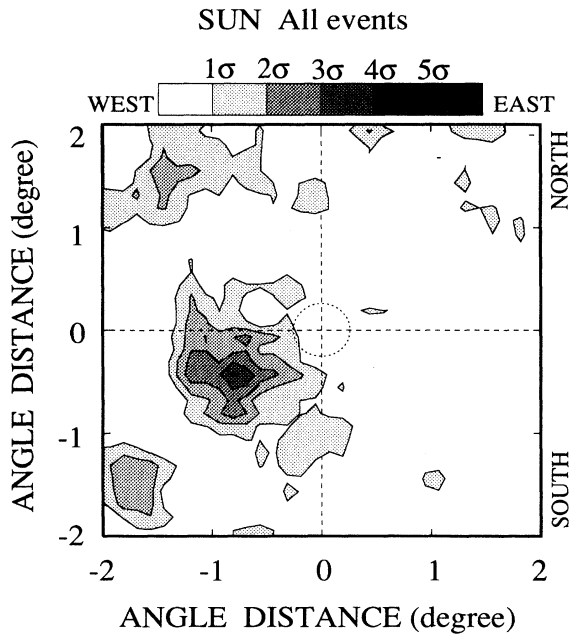

FIG. 4. Arrival direction of all events in the area of $4°\times4°$ centered on the Sun (the circle shown by the dotted line). The map gives the weight of deficit event density from the background, and contour lines start from a 1σ deficit with a step of 1σ.

The observed deflection of the Sun's shadow should be interpreted by the combined effect of the magnetic fields of the Sun, interplanetary space, and the Earth. A crude estimation for the effect of each magnetic field is as follows. Assuming that the solar magnetic field is a dipole with a strength of 1 G at the surface of the solar poles, a Monte Carlo simulation [16] shows that the Sun's shadow by 10-TeV protons is displaced by about 0.3°. Of course, the actual solar magnetic field is not a simple dipole and there is uncertainty about its magnetic-field configuration and its change, but this may give a measure of the deflection. The deflection in the geomagnetic field is estimated to be about 0.18° for 10-TeV protons (magnetic-field integral $\int B_\perp dl\sim1\times10^8$ G cm). The effect of the interplanetary magnetic field is very complicated. It has a sector structure and "garden-hose" field topology [17], with the field direction reversing across the sector boundary. The field strength near the Earth is known to be $(5-6)\times10^{-5}$ G and the garden-hose angle or stream angle is about 45° at the Earth's orbit. The Archimedes spiral configuration of magnetic-field lines is well explained by Parker's equations including the angular velocity of solar rotation and the solar wind velocity [17] and the effective value of the magnetic-field integral will be several times 10^8 G cm. The effect of this magnetic field would be larger than that of the geomagnetic or solar magnetic field. When the Sun is active, however, effects of changes in the solar wind velocity and the solar magnetic-field polarity will produce a large-scale disordered magnetic field. These also cause some effects on the cosmic-ray modulation. It is noted that the data set used in the present analysis was obtained in the period between 1990 and 1991 when the Sun was still in an active phase. Furthermore, the charge composition of the cosmic rays that produce air showers complicates somewhat the Sun's shadow [8]. Although complexities as well as uncertainties of the solar and interplanetary magnetic fields make it difficult to estimate the modulation

[1]The observed deficit of cosmic rays is less than expected (1321). The deficit within a circle of radius 2° centered on the maximum-likelihood position (0.86° W and 0.43° S) is about 35% of the expected one, while becoming about 70% within 3°. In short, the Sun's shadow may be fairly blurred by the magnetic deflection of cosmic rays in the space between the Earth and Sun. On account of this, the statistical significance obtained here is apparently smaller than expected ($\sim5\sigma$).

effects of cosmic rays quantitatively, it can be concluded that the observed deflection of the Sun's shadow is mostly caused by the magnetic-field effects between the Sun and Earth. The result seems to suggest that observation of the Sun's shadow, with a better statistics, may give a clue to investigate the large-scale structure and time variation of the interplanetary magnetic field or solar magnetic field.

The effect of the geomagnetic field is expected to be independently seen in the shadow of cosmic rays by the Moon. Same analysis was made for the Moon using the subset of all events, as shown in Fig. 5. Shown in this figure, together with the map of the event densities, are the deficit event densities on the belt of the width 1° along the right ascension (east-west direction) and the declination (south-north direction) as a function of the angle distance from the Moon center, respectively. A slight deviation of the shadow from the center is seen in this figure. As the profile of the Moon's shadow in the north-south direction is considered to be almost free from the effect of the geomagnetic field, the deviation of the highest deficit position from the center of the Moon gives an estimate of the systematic pointing errors of this array. It is then found to be about 0.1° from this figure.

On the other hand, the profile in the east-west direction is slightly affected by the geomagnetic field when the energies of cosmic rays are not so high. As seen in Fig. 5, the profile of the Moon's shadow is broadened in the east-west direction, with a systematic shift toward the west. The geomagnetic field would bend incident positively charged cosmic rays to make their apparent arrival direction shift to the west. The amount of the shift is also comparable with that expected. Same analysis using the subset of the events with $\sum\rho_{FT} > 100$ shows that a shift of the shadow is less than 0.1° in the north-south direction and about 0.14° to the west in the east-west direction. The geomagnetic effect still seems to make the shadow shift to the west, though its value is comparable to a systematic pointing error. Based on these results, the overall pointing error of the Tibet array is estimated to be smaller than 0.2°.

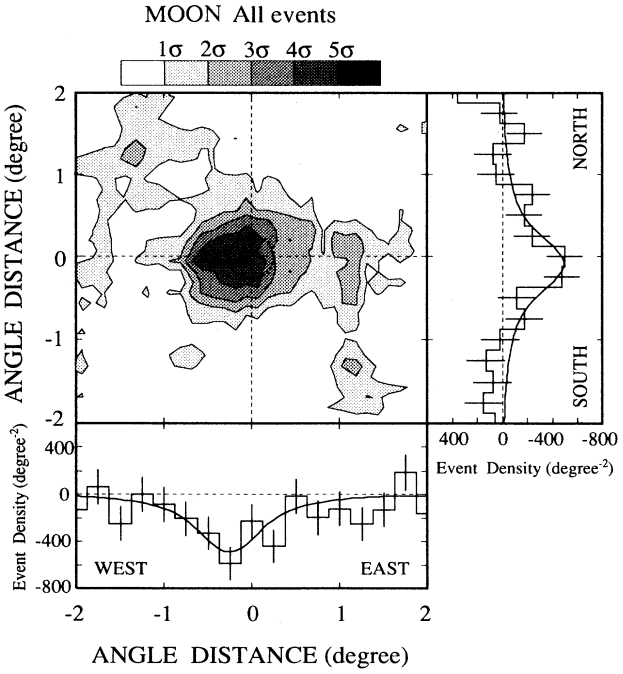

FIG. 5. Arrival direction of all events in the area of 4°×4° centered on the Moon as in Fig. 4. The circle shown by the dotted line stands for the Moon. Shown on the outside of the map are the deficit event densities against the angle distance from the Moon center on the belt of width 1° along the right ascension (west-east) and the declination (south-north). The solid curves show the event density distributions expected from the angular resolution of 0.87°.

IV. ANGULAR RESOLUTION

As discussed in Sec. II, the Monte Carlo simulation suggests that the angular resolution of the present Tibet array is 1.15° for proton showers with its mode energy 7 TeV. This resolution can be confirmed by the observation of the shadowing of cosmic rays by the Moon, since it is known to be sensitive to the shape of the event density distribution around the Moon.

The maximum-likelihood method was used to estimate the angular resolution. To use this method, an angular resolution function must be *a priori* introduced, and this can be well represented by the opening angle distribution between the given and estimated directions for simulated showers. However, since the experimental conditions for detecting showers are properly incorporated in the simulation, the opening angle distribution obtained is deformed from an ideal Gaussian distribution. We simply express this by a function composed of three two-dimensional Gaussian distributions, each function being G_i with a standard deviation σ_i, as

$$P_r(\theta)=\alpha G_1(\theta)+\beta G_2(\theta)+\gamma G_3(\theta)\ , \tag{2}$$

where $G_i(\theta)=1/2\pi\sigma_i^2 e^{-\theta^2/\sigma_i^2}$, θ is the opening angle between the given incident direction and the estimated one for the simulated shower, and α, β, and γ are the mixing parameters satisfying a relation $\alpha+\beta+\gamma=1$. The values of the parameter α, β, γ, and σ_i for proton-induced showers are summarized in Table II.

A fit of the above function to the Monte Carlo data for all events is presented in Fig. 6, with an angular resolution of 1.15°. In order to evaluate the angular resolution from the shape of the event density distribution around the Moon shown in Fig. 7, a scaled parameter R is introduced by replacing σ_i with $\sigma_i \times R/1.15°$ in Eq. (2). The value R reproducing the observed shadow gives the angular resolution of the array.

TABLE II. Summary of the parameter values for all events induced by protons, appearing in Eq. (2).

α	0.203	σ_1	0.38
β	0.444	σ_2	0.87
γ	0.353	σ_3	2.50

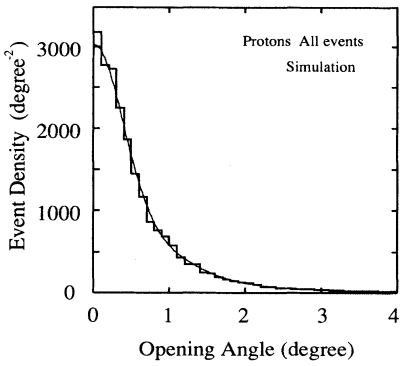

FIG. 6. Fit of the trial resolution distribution, composed of three two-dimensional Gaussian distributions, to the opening angle distribution of the Monte Carlo events obtained for the Tibet array. The distribution is the case for all events, with an angular resolution of 1.15°.

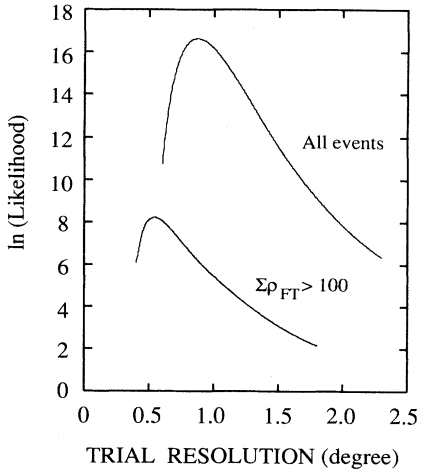

FIG. 8. Logarithm of the likelihood vs trial angular resolution R for the Moon data set. The upper curve is for all events and the lower one for those with $\sum\rho_{FT}>100$.

The likelihood function is the product of the differential probability as

$$\frac{dP}{dz} \propto \{N_{bg}(z)-\pi\theta_M^2 P_r(\theta(z),R)\} \tag{3}$$

for each event in the sample, where z is a scaled variable defined as

$$z=(1-\cos\theta)/(1-\cos\theta_{max}) ,$$

with $\theta_{max}=5.0°$, $N_{bg}(z)$ the normalized background function corresponding to Eq. (1), and θ_M the angle radius of the Moon.

The likelihood is computed numerically for many trial R's for the Moon data set; its natural logarithm is plotted against trial R in Fig. 8. The curves become maximum at $R=0.87°$ for all events and $R=0.54°$ for events with $\sum\rho_{FT}>100$, respectively. Let l_{max} be the natural logarithm of the likelihood at its maximum; the statistical significance of the deficit at the shadow is evaluated by

$$N_\sigma=\sqrt{2(l_{max}-l_\infty)} , \tag{4}$$

where l_∞ is the natural logarithm of the likelihood for a very large R [18]. The values of l_{max} and l_∞ are obtained to be 16.7 and 0.16 for all events and 8.2 and -0.58 for those with $\sum\rho_{FT}>100$, respectively. Using these data, we find $N_\sigma=5.8$ for all events and 4.2 for those with $\sum\rho_{FT}>100$, respectively. If the uncertainty in R is estimated to be the interval of R which the natural logarithm of the likelihood decreases by 0.5 from its maximum, corresponding to one standard deviation, then the angular resolution of the array is $0.87°^{+0.13°}_{-0.10°}$ for all events and $0.54°^{+0.11°}_{-0.08°}$ for those with $\sum\rho_{FT}>100$. These are consistent with those obtained by the simulation in Sec. II. The curves in Fig. 7 show the expected event densities obtained by using these values for angular resolutions.

CYGNUS [9] and CASA [10] assume a single two-dimensional Gaussian distribution to estimate the angular resolution. If we use this function in the likelihood analysis, then the fitted resolution of our array is obtained to be $0.63°^{+0.08°}_{-0.07°}$ for all events, though the statistical significance is 5.2σ for the shadow of the Moon. That is, the hypothesis of a single two-dimensional Gaussian resolution function would give a better angular resolution than the present analysis.

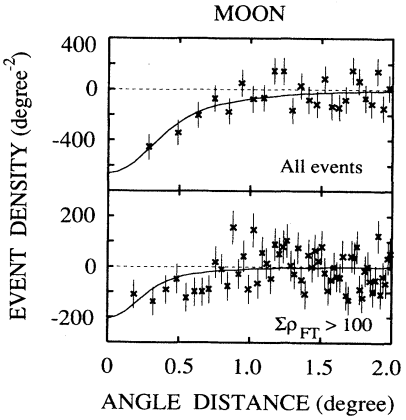

FIG. 7. Angular density of events vs angular distance from the center of the Moon. The data point shows the event density at each angle distance after background is subtracted. The solid curves show the expected event densities with an angular resolution of 0.87° for all events and 0.54° for those with $\sum\rho_{FT}>100$, respectively, obtained from the maximum-likelihood analysis.

V. CONCLUSIONS

The Tibet air-shower array at an altitude of 4300 m above sea level has been operated continuously since January, 1990. Using the shower data obtained with this array, the shadowing of the cosmic rays at energies around 10 TeV by the Moon and Sun has been examined to estimate the angular resolution of the array system. Data samples used for this analysis are 1.09×10^6 events for the Moon and 1.24×10^6 events for the Sun, within 8°

from each body and with the zenith angles less than 50°. The main results obtained are briefly summarized as follows:

(1) The shadowing of high-energy cosmic rays by the Moon has been observed at the 5.8σ level for the shower events with its mode energy 7 TeV.

(2) The shadow of the Sun by cosmic rays with its mode energy 7 TeV was observed in the direction away from the Sun by 0.86° to the west and 0.43° to the south, with a sufficient significance of the displacement. The statistical significance for the shadow at this position is 3.7σ, which is smaller than expected. It is considered that the combined effect of the magnetic fields between the Sun and Earth has been observed in the shadow of cosmic rays by the Sun. The geomagnetic deflection was also found in the shadow of the Moon.

(3) A detailed analysis on the shape of the Moon's shadow shows that the mean angular resolution of the Tibet array is $0.87°^{+0.13°}_{-0.10°}$ for the shower events with its mode energy 7 TeV and $0.54°^{+0.11°}_{-0.08°}$ for those with its mode energy 35 TeV. The systematic pointing error of the array is estimated to be smaller than 0.2°.

The results well confirm that the Tibet array is capable of observing air showers at energies around 10 TeV with an angular resolution better than 1°. High-angular-resolution observations of the cosmic-ray shadow of the Sun, with a better statistics, may produce new information on the large-scale structure of the interplanetary magnetic field in the near future.

ACKNOWLEDGMENTS

We are grateful to Professor J. Arafune of ICRR, University of Tokyo and Professor S. X. Fan of IHEP, Chinese Academy of Sciences for their support and encouragement. We also wish to thank the staffs of the Geothermal Power Station at Yangbajing in Tibet for allowing us to use every facility necessary for carrying out the experiment. This work was supported in part by Grants-in-Aid for Scientific Research and also for International Scientific Research from the Ministry of Education, Science and Culture, in Japan and the Committee of Natural Science Foundation in China.

[1] M. Samorski and W. Stamm, Astrophys. J. **268**, L17 (1983).

[2] T. C. Weekes, Space Sci. Rev. **59**, 315 (1992); D. J. Fegan, in *Proceedings of the 21st International Cosmic Ray Conference,* Adelaide, Australia, 1990, edited by R. J. Protheroe (Graphic Services, Northfield, South Australia, 1990), Vol. 11, p. 23.

[3] G. Vacanti *et al.*, Astrophys. J. **377**, 467 (1991).

[4] B. L. Dingus *et al.*, Phys. Rev. Lett. **60**, 1785 (1988).

[5] B. L. Dingus *et al.*, Phys. Rev. Lett. **61**, 1906 (1988).

[6] G. W. Clark, Phys. Rev. **108**, 450 (1957).

[7] M. Urban *et al.*, in *Astrophysics and Particle Physics,* Proceedings of the Topical Seminar, San Miniato, Italy, 1989, edited by G. Castellini *et al.* [Nucl. Phys. B (Proc. Suppl.) **14B**, 223 (1990)].

[8] J. Lloyd-Evans, in *Proceedings of the 19th International Cosmic Ray Conference,* La Jolla, California, 1985, edited by F. C. Jones, J. Adams, and G. M. Mason, NASA Conf. Publ. 2376 (Goddard Space Flight Center, Greenbelt, MD, 1985), Vol. 2, p. 173; J. Linsley, *ibid.*, Vol. 3, p. 465.

[9] D. E. Alexandreas *et al.*, Phys. Rev. D **43**, 1735 (1991).

[10] B. E. Fick *et al.*, in *Proceedings of the 22nd International Cosmic Ray Conference,* Dublin, Ireland, 1991, edited by M. Cawley *et al.* (The Dublin Institute for Advanced Studies, Dublin, Ireland, 1991), Vol. 2, p. 728.

[11] A. Karle *et al.*, in *Proceedings of the 22nd International Cosmic Ray Conference* [10], Vol. 4, p. 460.

[12] M. Amenomori *et al.*, Nucl. Instrum. Methods A **288**, 619 (1990); M. Amenomori *et al.*, in *High Energy Gamma-Ray Astronomy,* Proceedings of the Conference, Ann Arbor, Michigan, 1990, edited by James Matthews, AIP Conf. Proc. No. 220 (AIP, New York, 1990), p. 257; A. X. Huo *et al.*, in *Proceedings of the 21st International Cosmic Ray Conference* [2], Vol. 3, p. 427.

[13] Tibet ASγ Collaboration, M. Amenomori *et al.*, Phys. Rev. Lett. **69**, 2468 (1992).

[14] M. Nishizawa *et al.*, Nucl. Instrum. Methods A **285**, 532 (1989).

[15] K. Kasahara and S. Torii, Comput. Phys. Commun. **64**, 109 (1991).

[16] M. Ohnishi *et al.*, in *Proceedings of the 22nd International Cosmic Ray Conference* [10], Vol. 2, p. 69.

[17] E. N. Parker, *Interplanetary Dynamical Processes* (Interscience, New York, 1963).

[18] Particle Data Group, J. J. Hernández *et al.*, Phys. Lett. B **239**, 1 (1990).